

# Simultaneous control of orbital angular momentum and beam profile in two-mode polarization-maintaining fiber

ROBERT D. NIEDERRITER,<sup>1,\*</sup> MARK E. SIEMENS,<sup>2</sup> AND JULIET T. GOPINATH<sup>1,3</sup>

<sup>1</sup>Department of Physics, University of Colorado, 390 UCB, Boulder, Colorado 80309-0390, USA

<sup>2</sup>Department of Physics and Astronomy, University of Denver, 2112 East Wesley Avenue, Denver, Colorado 80208, USA

<sup>3</sup>Department of Electrical, Computer, and Energy Engineering, University of Colorado, 425 UCB, Boulder, Colorado 80309-0425, USA

\*Corresponding author: robert.niederriter@colorado.edu

Received 6 September 2016; revised 29 October 2016; accepted 30 October 2016; posted 2 November 2016 (Doc. ID 275259); published 12 December 2016

**We report simultaneous control of the orbital angular momentum (OAM) and beam profile of vortex beams generated in two-mode polarization-maintaining optical fiber. Two higher-order eigenmodes of the fiber are combined to form optical vortices. Reduced coherence between the fiber modes decreases the mode purity. Varying the coherence of the fiber modes changes the average OAM while maintaining a constant annular intensity profile. Additionally, a donut mode has been shown to be insensitive to bends and twists in the fiber.** © 2016 Optical Society of America

**OCIS codes:** (060.2310) Fiber optics; (060.2420) Fibers, polarization-maintaining; (080.4865) Optical vortices; (140.3300) Laser beam shaping; (260.6042) Singular optics.

<https://doi.org/10.1364/OL.41.005736>

Continuously tunable orbital angular momentum (OAM) (non-integer  $l$ ) is desirable for applications such as particle manipulation [1,2] and optical communications [3]. While tunable OAM beams have been generated, the change in OAM is typically accompanied by a change in the intensity profile [4–8]. Čižmár *et al.* have demonstrated continuous OAM tuning independent of the beam intensity profile by time-sharing two vortex beams of opposite helicity [2]. Cross-polarized non-interfering superpositions of Laguerre–Gaussian beams have also been used for particle manipulation [9]. These previous studies have used non-interfering combinations of free-space optical vortices, and we now extend this work to vortices in optical fiber. The generation and transport of OAM in fibers show promise for optical communications [10], superresolution imaging [11,12], sensing [13], and particle manipulation [14].

While the eigenmodes of conventional step-index fiber do not carry OAM, modes from the LP<sub>11</sub> group can be combined to generate vortex modes with  $l = \pm 1$  [15]. For example, OAM has been generated using annular core fiber [16] and stressed step-index fibers [17,18]. Recently, we demonstrated

continuously tunable OAM generation in polarization-maintaining (PM) optical fiber by varying the relative phase between the fiber eigenmodes [19]. While the average OAM was smoothly tunable between  $\pm 1 \hbar$  in that work, the beam profile also changed dramatically.

In this Letter, we use the temporal coherence between fiber modes to enable control of both the laser beam profile and OAM using an optical fiber. The OAM is tunable between  $+1$  and  $-1 \hbar$ /photon with a constant donut-shaped beam profile and constant power. Alternatively, the beam profile can be varied with constant OAM. Finally, both beam profile and OAM can have greatly reduced sensitivity to bending and twisting of the fiber. We present a significant innovation: separate tuning of both the OAM and the beam profile using optical fiber. The degree of temporal coherence and the relative phase between two fiber modes are used as two degrees of freedom that determine the average OAM and beam profile. Tuning these two parameters enables unprecedented separate control of the OAM and beam profile using optical fiber.

To begin, we analyze the effect of temporal coherence on the OAM generated using high-birefringence PM fibers. The eigenmodes of strongly birefringent ( $\Delta n > 10^{-4}$ ) circular waveguides have electric fields of the form [20,21]

$$\begin{aligned} E_l^{e,x} &= \hat{x}F_l(r) \cos(l\theta), & E_l^{o,x} &= \hat{x}F_l(r) \sin(l\theta), \\ E_l^{e,y} &= \hat{y}F_l(r) \cos(l\theta), & E_l^{o,y} &= \hat{y}F_l(r) \sin(l\theta), \end{aligned} \quad (1)$$

where  $F_l(r)$  describes the radial dependence,  $l$  is the angular mode index,  $r$  and  $\theta$  are the radial and azimuthal coordinates, and  $\hat{x}$  and  $\hat{y}$  indicate linear polarization along the fast and slow fiber axes. The superscripts  $e$  and  $o$  indicate even and odd angular dependence of the electric field.

The azimuthal structure of the higher-order ( $l > 0$ ) PM fiber modes contains combinations of OAM states, as  $\cos(l\theta) \propto \exp(il\theta) + \exp(-il\theta)$ . Combined PM fiber modes,  $E_l^{e,x} + \exp(i\Delta\phi)E_l^{o,x}$ , generate pure OAM states only if the relative phase between the component fiber modes is  $\Delta\phi = \pm\pi/2$  [19]. Such combination assumes there is a fixed phase relationship between the two fiber modes. In the general

case, there is some temporal delay,  $\tau$ , between the two fiber modes. The OAM and intensity depend on the temporal correlations between the two modes, described by the degree of coherence,  $\gamma(\tau)$  [22], in addition to the relative phase between the modes,  $\Delta\phi$ . The degree of temporal coherence is an additional parameter for control of the OAM generated in optical fiber.

Consider the combination of the even and odd eigenmodes of order  $l$  with the same polarization and amplitude. The electric field at the plane immediately after the fiber is the sum of the two modal fields,  $E_l^{e,x}$  and  $E_l^{o,x}$ , with some time delay,  $\tau$ . The time-dependent electric field of each mode is  $E(r, \theta)u(t)$ , where  $u(t)$  is a unit-amplitude function that contains the time dependence of the electric field.  $E(r, \theta)$  includes the transverse spatial dependence of the electric field:

$$E = F_l(r) \cos(l\theta)u(t) + F_l(r) \sin(l\theta)u(t + \tau). \quad (2)$$

We can write the electric field as a superposition of OAM modes,  $\exp(\pm il\theta)$ ,

$$E = \frac{F_l(r)}{2} \{e^{il\theta}[u(t) - iu(t + \tau)] + e^{-il\theta}[u(t) + iu(t + \tau)]\}. \quad (3)$$

Decomposing the field into OAM modes, the power in each  $\pm l$  mode is

$$P_{\pm l} = \left\langle \left| \iint e^{\mp il\theta} E dr d\theta \right|^2 \right\rangle = \frac{1}{4} \langle |u(t) \mp iu(t + \tau)|^2 \rangle. \quad (4)$$

We simplify the expression using the properties of  $u(t)$ . First,  $u(t)$  is normalized such that  $\langle |u(t)|^2 \rangle = \langle |u(t + \tau)|^2 \rangle = 1$ . Second, we identify the product as the complex degree of coherence:  $\gamma(\tau) = \langle u^*(t)u(t + \tau) \rangle$  [22]. The complex degree of coherence can be written as the product of amplitude and phase terms,  $\gamma(\tau) = \gamma(\tau) \exp(i\omega\tau)$ , where  $\omega$  is the mean angular optical frequency. We have assumed  $\omega\tau = \Delta\phi$  is the sole contribution to the temporal phase. Then the fractional power in each  $\pm l$  OAM state is

$$P_{\pm l} = \frac{1}{2} [1 \pm \gamma(\tau) \sin(\Delta\phi)]. \quad (5)$$

The average OAM is calculated from the power in each mode:

$$L_{\text{ave}} = \frac{\sum l P_l}{\sum P_l} = l\gamma(\tau) \sin(\Delta\phi). \quad (6)$$

The OAM oscillates as  $\sin(\Delta\phi)$  with amplitude  $l\gamma(\tau)$ . The electric field is correlated with itself over some time,  $\tau_c$ , known as the coherence time. For phase variations much smaller than the coherence time,  $\Delta\phi/\omega \ll \tau_c$ ,  $\gamma$  varies slowly compared to  $\sin(\Delta\phi)$  and  $\gamma$  can be approximated as constant. In this approximation, the sinusoidal amplitude and phase in Eq. (6) are independent.

For practical applications, there are several cases of interest. For a time delay between modes less than the coherence time,  $\tau \ll \tau_c$ ,  $\gamma(\tau) \approx 1$ , and the average OAM generated is equal to  $l \sin(\Delta\phi)$ . This pure  $\sin(\Delta\phi)$  dependence was reported in [19]. On the other hand, for  $\tau \gg \tau_c$ , the OAM oscillations become very small. The average OAM is approximately zero, but the time-average intensity profile is a donut. For a fixed relative

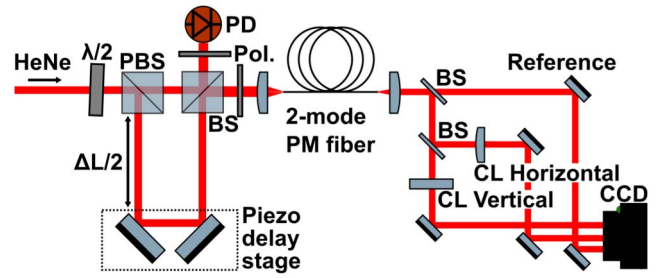


**Fig. 1.** Experimental schematic for generating OAM via mode addition in PM fiber. HeNe, helium–neon laser (632.8 nm);  $\lambda/2$ , half wave-plates; PBS, polarizing beam splitter; BS, non-polarizing beam splitter; PD, photodetector; Pol., polarizers; CL, cylindrical lens;  $\Delta L$ , delay length. The long delay length ( $\Delta L$  of zero to 45 cm) controls the degree of coherence,  $\gamma(\tau)$ . The piezo-driven translation stage varies an additional delay length of  $<2 \mu\text{m}$ , corresponding to a change in the relative phase between the fiber modes,  $\Delta\phi$ , of  $<5\pi$ . The polarizers are oriented at  $45^\circ$  to combine the horizontal and vertical polarizations with equal amplitudes. The cylindrical lenses Fourier transform the fiber output onto the plane of the CCD.

phase such that  $\sin(\Delta\phi) = 1$ , the OAM can be varied between 0 and  $l$  independently of the beam profile by varying the degree of coherence  $\gamma$ . Conversely, when the relative phase is fixed such that  $\sin(\Delta\phi) = 0$ , the beam profile can be varied independently of the average OAM.

We experimentally explore the impact of incomplete temporal coherence on OAM generation in PM fibers. The fiber used (PM980-XP, Nufern) has  $\sim 3.5 \times 10^{-4}$  birefringence and supports two mode groups at 633 nm. We separately excite the  $E_1^{e,x}$  and  $E_1^{o,x}$  fiber modes of the same polarization by off-axis coupling (Fig. 1). One incident beam is offset slightly from the fiber axis in the horizontal direction to selectively couple into a single fiber mode. The second incident beam is offset slightly in the vertical direction to couple into the complementary fiber mode. Each input beam is separately aligned to optimize the fiber output. The individual fiber modes are observed to be stable in power and shape when bending and heating the fiber, indicating these are the eigenmodes. The two fiber modes have the same polarization and travel at nearly the same rate through the 2 m fiber. Assuming no contribution from bending stress, we estimate less than 10 fs/m difference in the propagation time due to slight differences in the propagation constant. This small time delay is constant for a given fiber configuration during our experiments. In contrast, modes of opposite polarization would experience a larger time delay of 1.17 ps/m due to the fiber birefringence.

The time delay,  $\tau$ , between the two fiber modes is controlled by introducing a long path delay,  $\Delta L$ , between zero and 45 cm, into one beam. For the HeNe beam used in these experiments, this range of delays corresponds to degrees of temporal coherence between 1 and 0.08. A piezo-driven translation stage controls a short additional delay length ( $<2 \mu\text{m}$ ) that varies the relative phase between the fiber modes ( $<5\pi$ , measured using interference on a photodiode). The additional time delay between modes due to the piezo motion ( $\sim 5$  fs) is much smaller than the coherence time of the HeNe ( $\sim 1$  ns), so the degree of coherence,  $\gamma(\tau)$ , is approximately constant during these relative phase scans.

The output beam profile is measured with a CCD. The beam also passes through horizontally and vertically focusing cylindrical lenses to measure the average OAM [19,23]. Passing through a cylindrical lens causes a beam with OAM to rotate [24]. The amount of rotation is quantified by the  $xy$ -covariance [19,23,24],

$$\langle xy \rangle = \frac{\iint I(x, y)(x - \langle x \rangle)(y - \langle y \rangle) dx dy}{\iint I(x, y) dx dy}, \quad (7)$$

where  $(x, y)$  are Cartesian coordinates,  $I(x, y)$  is the laser intensity distribution, and  $(\langle x \rangle, \langle y \rangle)$  is the location of the beam centroid.

In addition to the OAM, the beam divergence also affects the  $xy$ -covariance, which needs to be carefully calibrated when measuring the OAM with a single cylindrical lens [24]. For this work, we use a pair of cylindrical lenses oriented with orthogonal axes, eliminating any systematic offset due to the beam divergence. The average OAM is proportional to the difference in the  $xy$ -covariances of the beam a distance  $d$  after horizontal and vertical cylindrical lenses of focal length  $f$  [19,23]:

$$L_{\text{ave}} = \hbar \frac{2\pi f}{\lambda d^2} (\langle xy \rangle_v - \langle xy \rangle_h), \quad (8)$$

where  $\lambda$  is the wavelength and subscripts  $v$  and  $h$  correspond to the vertically and horizontally focusing cylindrical lenses, respectively. The CCD is placed one focal length from the cylindrical lenses ( $d = f$ ) and records the three beams simultaneously.

Figure 2 shows the measured average OAM as a function of the relative phase,  $\Delta\phi$ , at four degrees of coherence  $\gamma(\tau)$ , as controlled by the long delay  $\tau = \Delta L/c$ . The long delay,  $\tau = \Delta L/c$ , controls  $\gamma(\tau)$ , while the short piezo-controlled delay controls  $\Delta\phi$ . The average OAM oscillates as a function of the

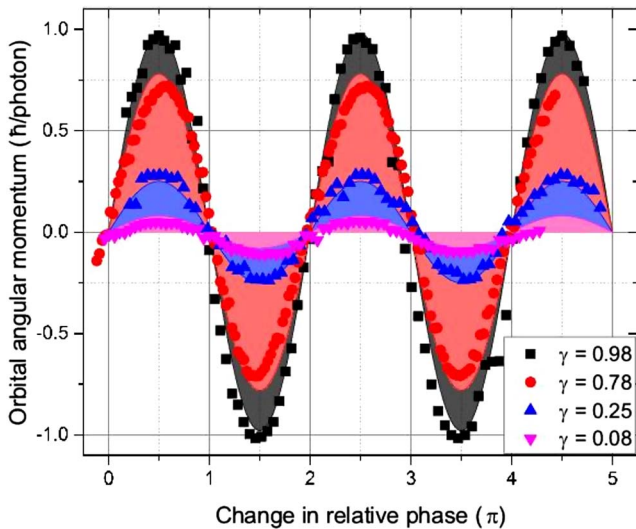


**Fig. 2.** Average OAM per photon as a function of the relative phase between fiber modes. Four different delay lengths,  $\Delta L$ , were used, corresponding to different degrees of coherence,  $\gamma$ . All four datasets have a period of  $2\pi$ , within the phase measurement uncertainty, and the peak-to-peak OAM depends on the coherence. The OAM measurement uncertainty is  $0.006 \hbar/\text{photon}$ , twice the standard deviation of 31 repeated measurements. The shaded curves are predictions calculated from Eq. (6) with  $l = 1$  and the same value of  $\gamma$  as each dataset.

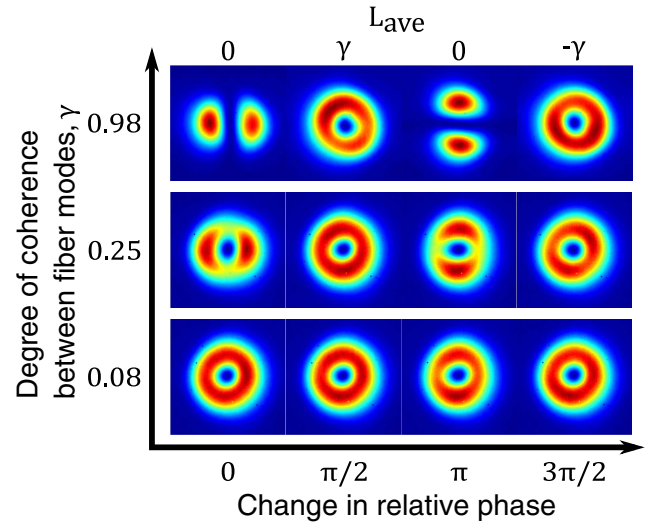


**Fig. 3.** Measured beam profiles corresponding to the degree of temporal coherence,  $\gamma$ , and relative phase between PM fiber modes, modulo  $2\pi$ . The average OAM,  $L_{\text{ave}}$ , of each column is listed at the top. For  $\gamma \approx 1$ , the intensity pattern changes between donut and two-lobed shapes depending on the relative phase. As the temporal coherence between modes decreases, the beam profile depends less on the relative phase. For  $\gamma \ll 1$ , the beam profile is insensitive to the relative phase.

phase delay,  $\Delta\phi$ , with period of  $2\pi$ . The amplitude of OAM oscillations decreases as a function of the temporal coherence,  $\gamma$ . Predictions calculated from Eq. (6) with the listed values of  $\gamma$  are shown as shaded curves. The measurement uncertainty in each OAM measurement is  $0.006 \hbar/\text{photon}$ .

The beam shape also depends on both the relative phase and temporal coherence between the fiber modes. Figure 3 shows the impact of these two knobs on the beam profile at the output of the fiber. When  $\gamma \approx 1$ , the beam profile oscillates with  $\Delta\phi$  between donut and two-lobed shapes while the OAM varies between  $\pm 1$ . With reduced  $\gamma$ , the changes in the intensity are suppressed. With  $\gamma \approx 0.08$ , there is little change in the beam profile as a function of the relative phase, and the OAM varies only between  $\sim \pm 0.08$ .

When  $\Delta\phi = \pm\pi/2$ , the annular beam profile is independent of the temporal coherence. By adjusting  $\gamma$ , the OAM can be varied with a constant beam profile. To show the independence of the beam shape and the OAM, Fig. 4 compares the horizontal cross sections of the donut beams with  $\Delta\phi = 3\pi/2$  and varying  $\gamma(\tau)$ . Each image was individually normalized to the peak intensity. The beam cross sections are qualitatively identical, showing that the OAM can be varied separately from the beam shape. In contrast, when  $\Delta\phi = m\pi$  (for integer  $m$ ), the average OAM is zero for any value of the coherence. The beam profile can be changed continuously between two-lobed and donut shapes. For low temporal coherence,  $\gamma \ll 1$ , the beam profile and average OAM are both independent of the relative phase between modes.

We have observed annular beams transmitted through the fiber undisturbed by fiber bending when the degree of temporal coherence was low. With  $\gamma \approx 1$ , the fiber was bent gently by hand to cause oscillations in the beam profile, similar to the top row of images in Fig. 3. Then the same bending was repeated with  $\gamma \approx 0.08$ . When the temporal coherence was low, bending

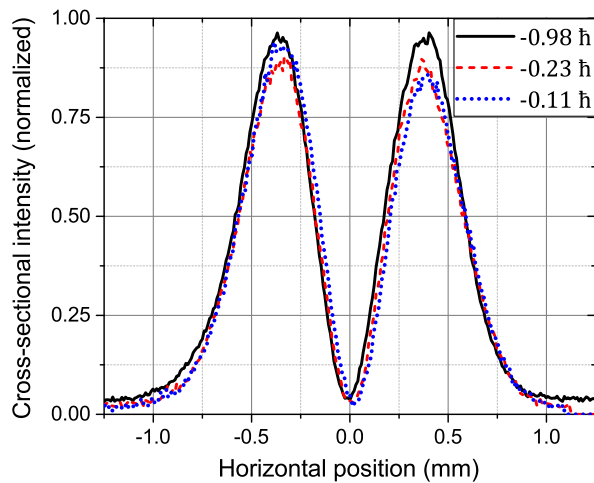


**Fig. 4.** Horizontal beam cross sections for three degrees of temporal coherence,  $\gamma$ , with relative phase  $\Delta\phi = 3\pi/2$  (right-hand column of Fig. 3). The intensity pattern is constant while the average OAM is changed by varying the degree of temporal coherence.

produced negligible changes in the beam profile, similar to the bottom row of Fig. 3. A bend-insensitive donut beam could be easily generated using a laser with low temporal coherence, such as an amplified spontaneous emission source or laser diode. Short path length differences of a few millimeters or centimeters would extinguish the correlation between the electric fields.

In general, the degree of temporal coherence could be controlled completely independently of the relative phase between two beams. In these experiments, a time delay was a straightforward means to control both the temporal coherence and the relative phase. In future work, the spectral bandwidth of the laser source could be used to vary the temporal coherence while a delay stage controls  $\Delta\phi$ . With a small, fixed delay length, increasing the spectral bandwidth of the laser source would decrease the degree of temporal coherence. For example, the relative phase could be maintained at  $\Delta\phi = \pi/2$  with active feedback; from Eq. (6), the OAM is then directly proportional to  $\gamma$  and would be tunable by adjusting the spectral bandwidth of the laser source.

We have shown that the temporal coherence is a crucial parameter determining the OAM generated in optical fibers. Incomplete temporal coherence decreases the maximum OAM generated by fiber mode combinations. Adjusting the degree of coherence and the relative phase between modes enables simultaneous control over the average OAM and beam profile. The average OAM is continuously tunable without affecting the annular profile, with applications in particle manipulation and lithography [25]. Using temporally incoherent fiber modes, a donut-shaped beam with zero average OAM could be insensitive to bending and twisting of the fiber, with potential to enable fiber-coupled superresolution imaging. The observed benefits and challenges of imperfect temporal coherence are relevant to all applications of transmitting and generating OAM modes in optical fibers.

**Funding.** National Science Foundation (NSF) (ECCS 1509733, ECCS 1509928, DMR 1553905, ECCS 1554704); U.S. Department of Defense (DOD).

**Acknowledgment.** The authors are grateful for technical discussions with Dr. Martin Lavery (University of Glasgow), Samuel Alperin (University of Denver), Trystan Binkley-Jones, and Brendan Heffernan (University of Colorado Boulder) as well as loans of a vortex phase plate from Dr. Stephanie Meyer and Dr. Emily Gibson (University of Colorado Denver, Anschutz Medical Campus) and a wavefront sensor from Dr. Robert McLeod (University of Colorado Boulder).

## REFERENCES

1. S. H. Tao, X.-C. Yuan, J. Lin, X. Peng, and H. B. Niu, *Opt. Express* **13**, 7726 (2005).
2. T. Čižmár, H. I. C. Dalgarno, P. C. Ashok, F. J. Gunn-Moore, and K. Dholakia, *Appl. Phys. Lett.* **98**, 081114 (2011).
3. P. Gregg, P. Kristensen, A. Rubano, S. Golowich, L. Marrucci, and S. Ramachandran, in *Conference on Lasers and Electro-Optics* (Optical Society of America, 2016), paper JTh4C.7.
4. M. S. Soskin, V. N. Gorshkov, M. V. Vasnetsov, J. T. Malos, and N. R. Heckenberg, *Phys. Rev. A* **56**, 4064 (1997).
5. M. Soljačić and M. Segev, *Phys. Rev. Lett.* **86**, 420 (2001).
6. I. D. Maleev and G. A. Swartzlander, *J. Opt. Soc. Am. B* **20**, 1169 (2003).
7. C. H. J. Schmitz, K. Uhrig, J. P. Spatz, and J. E. Curtis, *Opt. Express* **14**, 6604 (2006).
8. G. Parisi, E. Mari, F. Spinello, F. Romanato, and F. Tamburini, *Opt. Express* **22**, 17135 (2014).
9. O. Brzobohatý, V. Karásek, T. Čižmár, and P. Zemánek, *Appl. Phys. Lett.* **99**, 101105 (2011).
10. A. E. Willner, H. Huang, Y. Yan, Y. Ren, N. Ahmed, G. Xie, C. Bao, L. Li, Y. Cao, Z. Zhao, J. Wang, M. P. J. Lavery, M. Tur, S. Ramachandran, A. F. Molisch, N. Ashrafi, and S. Ashrafi, *Adv. Opt. Photon.* **7**, 66 (2015).
11. M. Gu, H. Kang, and X. Li, *Sci. Rep.* **4**, 3627 (2014).
12. L. Yan, P. Gregg, E. Karimi, A. Rubano, L. Marrucci, R. Boyd, and S. Ramachandran, *Optica* **2**, 900 (2015).
13. R. D. Niederriter, M. E. Siemens, and J. T. Gopinath, in *Conference on Lasers and Electro-Optics (CLEO)* (Optical Society of America, 2015), paper SM1L.5.
14. T. Čižmár and K. Dholakia, *Nat. Commun.* **3**, 1027 (2012).
15. S. Ramachandran and P. Kristensen, *Nanophotonics* **2**, 455 (2013).
16. N. Bozinovic, S. Golowich, P. Kristensen, and S. Ramachandran, *Opt. Lett.* **37**, 2451 (2012).
17. D. McGloin, N. B. Simpson, and M. J. Padgett, *Appl. Opt.* **37**, 469 (1998).
18. S. Li, Q. Mo, X. Hu, C. Du, and J. Wang, *Opt. Lett.* **40**, 4376 (2015).
19. R. D. Niederriter, M. E. Siemens, and J. T. Gopinath, *Opt. Lett.* **41**, 3213 (2016).
20. A. W. Snyder and J. D. Love, *Optical Waveguide Theory* (Chapman & Hall, 1983).
21. A. N. Alekseev, A. V. Volyar, and T. A. Fadeeva, *Tech. Phys. Lett.* **31**, 374 (2005).
22. J. W. Goodman, *Statistical Optics* (Wiley, 2000).
23. J. Serna, F. Encinas-Sanz, and G. Nemes, *J. Opt. Soc. Am. A* **18**, 1726 (2001).
24. S. N. Alperin, R. D. Niederriter, J. T. Gopinath, and M. E. Siemens, *Opt. Lett.* **41**, 5019 (2016).
25. T. F. Scott, B. A. Kowalski, A. C. Sullivan, C. N. Bowman, and R. R. McLeod, *Science* **324**, 913 (2009).